Journal of the Korean Ceramic Society (2024) 61:837–853
https://doi.org/10.1007/s43207-024-00398-6

ORIGINAL ARTICLE

Structural and antibacterial activity of developed nano-bioceramic DD3/ZrO2/ZnO/CuO powders

Dikra Bouras[1] · Mamoun Fellah[2,3] · Majeed Ali Habeeb[4] · Lamia Aouar[5] · Regis Barille[6] · Gamal A. El-Hiti[7]

Received: 17 January 2024 / Revised: 9 March 2024 / Accepted: 24 March 2024 / Published online: 6 May 2024

Abstract

Ceramic materials based on mullite, cristobalite, and zircon phases prepared with different zinc and copper additions using the co-precipitation method and followed by calcination at 500 °C for 2 h are investigated. The effectiveness of these substrates against bacteria was tested against Gram-positive and Gram-negative pathogenic strains: *Staphylococcus aureus*, *Bacillus subtilus*, *Escherichia coli*, *Pseudomonas putida,* and *Enterobacter aerogenes*. The obtained nanoparticles with different crystal sizes were subjected to various types of characterization, including structural by X-ray diffraction (XRD), morphology by scanning electron microscopy (SEM), energy dispersive spectroscopy (EDS) transmission electron microscopy (TEM), optical analysis by Raman spectroscopy. SEM images showed a change in the shape of the ceramic nanocomposites after adding zinc and copper to become similar to flake structures. This addition was detected by EDS analysis, where the first sample was found to contain 1.49 at.% Cu and 7.41 at.% Zn. The TEM image confirmed that the kaolin grains were in the form of nanotubes and were coated with spherical nanograins after adding ZrO_2, Zn, and Cu. The newly developed ceramic compound, consisting of mullite–zircon–zinc oxide–copper oxide with a primary source, kaolin DD3, was found to be more effective than its predecessors. It gave unprecedented anti-activity for many types of bacteria (Gram-positive and Gram-negative). Given the shape flake-like of the new ceramic compound, it provides a wider effective area through micro-tubes to the granules. It has a high percentage of holes that allow bacteria to be attracted and placed inside. A maximum inhibition zone of 38.1 ± 0.1 mm was obtained with *S. aureus* for DD3 + ZrO_2/ZnO (28 wt.%)/CuO (2.8 wt.%), a zone of 29.2 ± 0.2 mm with *P. putida*; for DD3 + ZrO_2/ZnO (14.28 wt.%)/CuO (5.37 wt.%) and an inhibition zone of 28.85 ± 0.15 mm was obtained with *B. subtilis* for DD3 + ZrO_2/ZnO (14.28 wt.%)/CuO (5.37 wt.%). The ceramic DD3 + 38% ZrO_2 possesses 33% of the holes, which represents the largest percentage in this compound and, therefore, is primarily responsible for the effect that occurs during biological application. All samples showed a high antibacterial activity, which increased with the addition of Zn:Cu and decreased with the increase in grain size. Ions and reactive oxygen species (ROS) release released into the cellular environment present a huge obstacle to dynamic membrane transport and lead to DNA damage and, ultimately, cell necrosis or apoptosis, which was effective for the inhibition of bacterial growth.

Keywords DD3/ZnO/CuO · DD3 + 38wt.% ZrO_2/ZnO/CuO · Antibacterial activity; (Zr^{4+}/Al^{3+}/Si^{4+}/Zn^{2+}/Cu^{2+}) ions · *Staphylococcus aureus* · *Bacillus subtilus* · *Pseudomonas putida*

✉ Dikra Bouras
bouras.dhikra@yahoo.fr

[1] Department of Science of Matter, Faculty of Science and Technology, Mohamed Cherif Messaadia University, Souk-Ahras, Algeria

[2] Mechanical Engineering Department, ABBES Laghrour University, PO 1252, CP 40004 Khenchela, Algeria

[3] Biomaterial, Synthesis and Tribology Research Team, ABBES Laghrour-University, PO 1252, CP 40004, Khenchela, Algeria

[4] Department of Physics, College of Education for Pure Sciences, University of Babylon, Babil, Iraq

[5] Department of Nature and Life Sciences, Larbi Ben M'hidi University, BP 358, 04000 Oum El Bouaghi, Algeria

[6] MOLTECH-Anjou, Université d'Angers/UMR CNRS 6200, 2 Bd Lavoisier, 49045 Angers, France

[7] Department of Optometry, College of Applied Medical Sciences, King Saud University, Riyadh 11433, Saudi Arabia

1 Introduction

Recently, eliminating microorganisms (pathogenic species, spoilage flora) that come into close touch with or approach the receiver surface has been a favored tactic to prevent microbial contamination [1, 2]. It is well-known that fungi and bacteria can lead to serious health issues for the general public in a number of industries, including the food business, biomedical, and surgical [3]. The increased interest in the field of research devoted to enhancing surface hygiene is justified by the necessity of combating surface colonization in these strategically important sectors [4].

The science of creating, manufacturing, and using structures and equipment with one or more components that are 100 nm (or a billionth of a millimeter) or smaller is known as nanotechnology [5]. In addition, they are utilized in textiles, coatings, food and energy technology, sunscreens, cosmetics, and a few pharmaceutical and medicinal items [6].

Bacteria are ubiquitous microorganisms present in our environment in soil, water, and air. Some bacteria are undoubtedly useful, while others are hazardous and can be deadly. They are considered to be the most common causes of the disease and lead to fatalities such as cancer and food poisoning [7]. Humans use many antimicrobial agents to fight harmful bacteria.

The discovery of antibiotics in the 1940s saved the lives of millions of people with infectious diseases. However, some bacteria have acquired resistance to these drugs [8, 9]. For this reason, scientists look for any natural or synthetic substance able to destroy microorganisms or prevent their proliferation [10, 11], in particular, with the development of surfaces able to prevent bacterial adhesion and inhibit microorganisms.

In this goal, the study of nanoparticles is a field of research in full expansion that deals with technological developments in the elaboration and characterization of new materials with possible applications to prevent bacterial contaminations. Considerable efforts developed in recent years have made it possible to establish the antimicrobial properties of some nanoparticles [12]. Zinc and copper oxides (ZnO and CuO) particles are among the most common inorganic substances in the fight against bacteria. They exhibit strong resistance to microorganisms due to their small size [13–15], which allows the creation of reactive oxygen species (ROS: $^{\cdot}O2^{-}$, $^{\cdot}OH$, and H_2O_2) on the surfaces of oxides.

These compounds have been selected because the human body contains these basic mineral elements as oligo-elements. They possess a very high specific surface, low band gap energies (3.4 eV for ZnO and 1.2 eV for CuO) [16–18], a potent antibacterial activity with small amounts, a high photocatalytic activity under ultraviolet light and a significant effect for biological applications [19–21]. The metal oxide surfactant and its nature have an influential role in organic conversions. All these properties have been characterized by previous research, and the role of metal ions in the increase of antimicrobial activity has been highlighted [20, 22].

The current study indicates the production of new products with antimicrobial activity based on an area in the city of Guelma in northeastern Algeria, where kaolin was extracted and used as a primary raw material. This kaolin-type material (denominated DD3) consists mainly of silicium and aluminum oxides and also contains very important proportions of organic matter such as K, Ca, Fe, and Mn [23]. Up until now, very few researchers have focused on the use of ceramic-type material to produce active components that have antimicrobial activity. With the goal of increasing the stimulation against bacteria, zirconium oxide (ZrO_2) was added to one of the obtained ceramic samples.

Therefore, the two types of ceramics (with and without ZrO_2) were treated at a temperature of 1300 ºC to obtain mullite–cristobalite for DD3 and mullite–zircon for DD3 + 38% of zirconia (ZrO_2) nanoparticles have recently shown promising results in the elimination of cancer cells and control of infections [24]. The use of zirconia showed a greater efficiency compared to a material without treatment. Moreover, the obtained inorganic materials have attractive, interesting properties because of their good thermal resistance, IR transparency, superior durability, less toxicity, safety, stability, and excellent selectivity [25, 26].

A new ceramic compound was used for the first time as an antibacterial, which proved its effectiveness on all types of bacteria used. This work aimed to analyze the effect of ceramic materials with new compounds (mullite–cristobalite and mullite–zircon) that show antibacterial properties due to their modification with zinc and copper oxides.

This was prepared using the co-precipitation method. During this, the particle size of the compound was reduced to 13–24 nm while nano-spherical shapes were obtained. The disc diffusion technique was used on Mueller–Hinton medium in Petri dishes. The synthesis of DD3-clay/CuO/ZnO and DD3Z + 38 wt% ZrO_2-clay/CuO/ZnO particles, their antibacterial activity, and their antibacterial action mechanism were studied. The inhibition zone for the DD3 sample reached 13.1 ± 0.1 mm for *P. putida*, 23.025 ± 0.07 mm for *S. aureus*, and 22.33 ± 0.32 mm for *B. subtilis*.

For samples DD3/ZnO (28 wt.%)/CuO (2.8 wt.%) and DD3Z/ZnO (28 wt.%)/CuO (2.8 wt.%), there was a significant improvement with the addition of (ZnO/CuO), which gave an average area of inhibition of 20.975 ± 0.02 and 38.1 ± 0.1 mm against *S. aureus*, respectively. The addition of (14.28 wt.% ZnO/5.37 wt.% CuO) average area of

inhibition *S. aureus* it arrived 32.525 ± 0.47 nm for DD3-clay and 37.25 ± 0.25 nm for DD3Z + 38 wt% ZrO_2-clay. Moreover, the prepared ceramic nanoparticles have been shown to have a positive effect on *Staphylococcus aureus*, a bacterium whose drug resistance has now increased significantly.

2 Experimental methods

Zn and Cu oxide particles were added differently to two distinct types of ceramic materials (DD3-clay and DD3 + ZrO_2-clay) to create antibacterial materials using the co-precipitation process. DD3 is a locally produced clay substance made of kaolin that is sourced from the Guelma (Djebel Debagh) region of Algeria and supplied by ETER, a ceramic manufacturer situated in Guelma. With CaO (0.38 wt%), Fe_2O_3 (0.64 wt%), MgO (0.06 wt%), and MnO (0.41 wt%), the primary constituents of DD3 clay are silica (SiO_2) and alumina (Al_2O_3). Three-eight percent zirconium oxide (ZrO_2; 99.5% purity) is added to the ceramic-based material mixture.

After silica is consumed in the vitreous phase, zirconium oxide (ZrO_2) is present and causes the development of zircon ($ZrSiO_4$) with a high rate of open porosity. The highest rate of porosity (33%) On the ceramic surface is achieved by adding 38 wt% ZrO_2 to DD3 clay, according to a recent study [25]. The DD3 and DD3 + 38% ZrO_2 powders were treated at a temperature of 1300 °C after grinding and sieving. The obtained ceramic powder was a composite of mullite–cristobalite (called DD3) and milling–zircon (called DD3Z) after this thermal transformation, according to the steps described in Fig. 1.

Following a heat treatment at 1300 ºC, the ceramic materials were mixed with 40 ml of distilled water (H_2O) to create the samples. The zinc acetate ($Zn(CH_3COO)_2.2H_2O$)

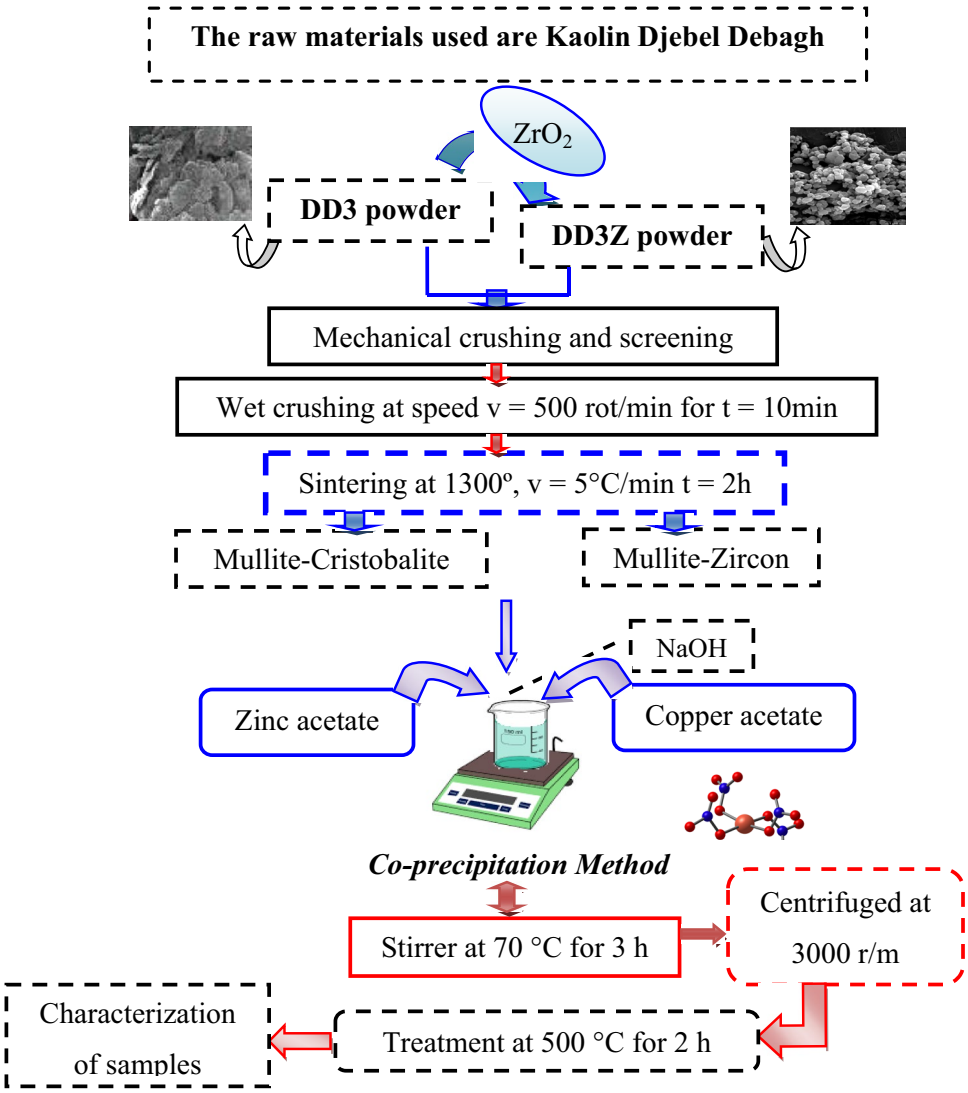

Fig. 1 Materials synthesis protocol and experimental parameters

(14.28%/28%), copper acetate ($Cu(CH_3COO)_2$) (2.8%/5.37%), and sodium hydroxide (NaOH) were added. These percentages were deliberately selected in light of the effectiveness of the findings regarding the photosynthetic process in relation to the thin-layered ceramic samples (zinc and copper).

The same ingredients were transformed into the ratios above to work with them as powders. After that the magnetic stirrer was used to mix the mixture at 70 °C for 3 h. Following the removal of the solvent, the product underwent a water wash, a 3000 r/m centrifugation, and 10 min of oven drying at 200 °C. After that, the process was calcined for 2 h at 500 °C to create ZnO and CuO nanocrystals. Figure 1 illustrates the various phases of nanocomposites' synthesis.

2.1 Antibacterial activity

Pathogenic bacteria: *Staphylococcus aureus* (ATCC 25923), *Bacillus subtilus* (ATCC 6633), *Escherichia coli* (ATCC: 25,922), *Pseudomonas putida* (ATCC 12633) and *Enterobacter aerogenes* (ATCC 13048) used in this investigation were obtained from a hospital's biological service (Oum El Bouaghi, Algeria. Bacterial stock cultures were kept on nutrient agar slants and kept cold (4 °C). To test the strains' antibacterial properties, they were cultured on nutrient agar plates for 18 h at 37 °C (Fig. 2).

Samples of mullite–cristobalite and mullite–zircon (10 mg) were dissolved in 10 ml of dimethyl sulfoxide (DMSO 10%), giving stock solutions of a 1 mg/ml concentration. Sterile paper discs (Whatman No. 1) of 8 mm diameter were saturated with 20 µl of the sample (1 mg/ml).

To evaluate the inhibitory effect of the two ceramic-type samples on bacterial growth, the Kirby Bauer method, which is routinely used in clinical laboratories for anti-biograms, was carried out [27, 28]. For each test strain, a suspension was prepared from one bacterial colony (18 h) in 2.5 ml of physiological water. A spectrophotometer adjusted the final concentration of the suspensions at 620 nm to reach 10^8 cells/cm^3.

The dried discs were then placed on the Muller Hinton agar already inoculated with the pathogenic strain. Ceramic pellets were then incubated at 37 °C for 24 h, and the inhibition zone was measured. All tests were performed in triplicates. The obtained data were statically analyzed using an unpaired *t* test with GraphPad Prism. The values were presented as the mean ± SD.

2.2 Examining data statistically

Using XL Stat (23.2.1141; Addinosoft SAS), the data were analyzed using repeated measures with two-way analysis variance (ANOVA) and the Tukey test for the least significant difference.

3 Results and discussion

3.1 X-ray diffraction

Figure 3a, b shows the XRD characterization for raw materials. It is observed that the first three most important peaks (24.85°, 19.85° and 12.30°) for ceramic samples are peaks of both kaolinite and halosite compounds, which confirms that the raw materials used are kaolinite (Fig. 3a). With the addition of 38% of ZrO_2 (Fig. 3b), it was confirmed that all the diffraction peaks correspond to zirconium single-edged structure (ASTM 37–1484).

The results of the XRD (Bruker AXS-D8) analysis of the DD3 and DD3 + ZrO_2 powders were heated to 1300 °C shows that the high-temperature treatment consists of three

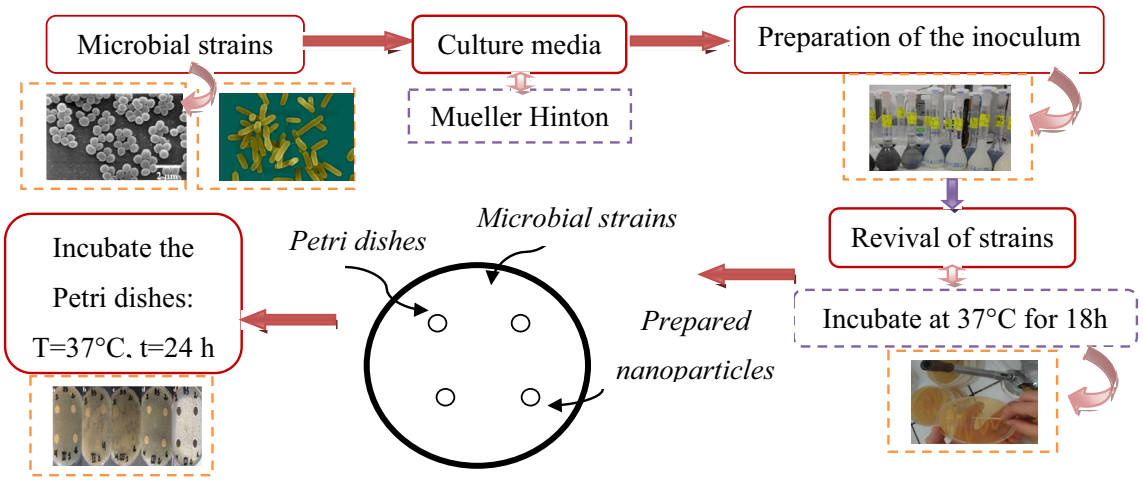

Fig. 2 Diffusion methods in agar medium (Antibiotic + nanoparticle)

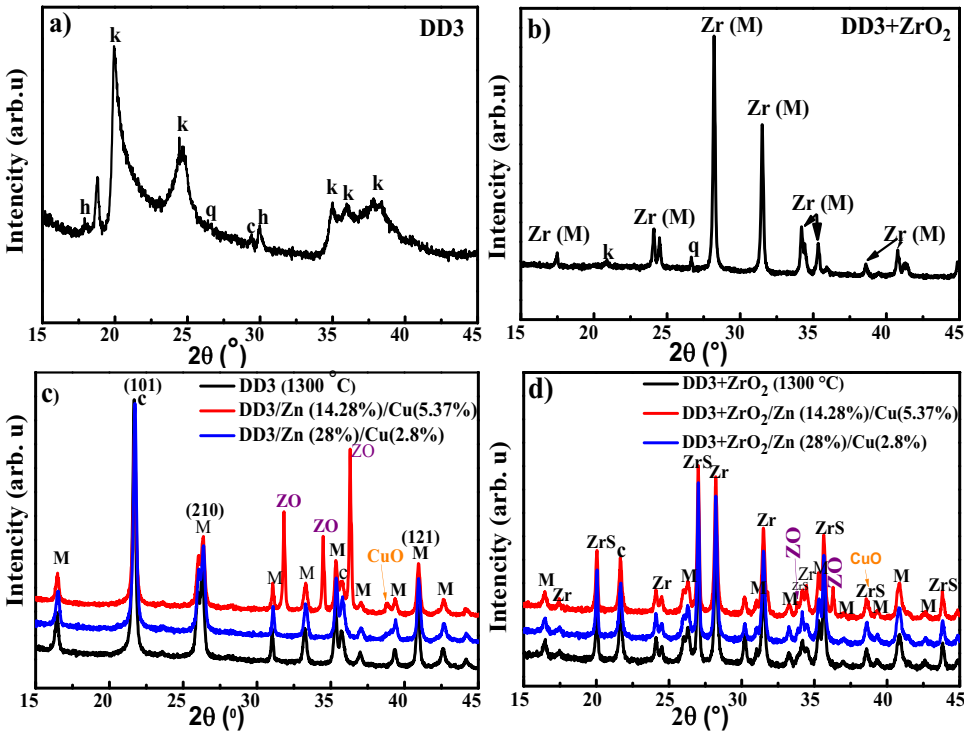

Fig. 3 XRD patterns of samples before treatment of **a** DD3; **b** DD3 + ZrO_2; and after treatment of: **c** DD3 + Zn/Cu; d) DD3 + ZrO_2/Zn/Cu. *K* kaolinite, *h* halosite, *q* quartz, *ZrS* Zircon ($ZrSiO_4$), *Zr* Zirconia (ZrO_2), *C* Cristobalite (SiO_2), *M* mullite ($3Al_2O_3.2SiO_2$), *ZO* zinc oxide (ZnO)

phases (Fig. 3c, d): the cristobalite phase (JCPDS 01-0424), the mullite phase (JCPDS 15–0776) and the zircon phase (JCPDS 06-0266). In addition to the essential phases and after the increase of zinc and copper compounds by a co-precipitation method, new peaks appeared at 31.80º, 34.46º and 36.29º. The latter correspond to the planes (100) (002) and (101), respectively, of the ZnO hexagonal wurtzite phase (JCPDS 36-1451). A distinct smaller peak is present at 38.78° corresponding to the planes (111) of the monoclinic phase of CuO (JCPDS 01–1117).

The size of the crystallite grains (D) for the materials obtained by the co-precipitation method (Fig. 3c, d) decreases when the Zn and Cu concentrations are increased, as shown in Table 1.

The sizes calculated with the Scherer's formula [29]:

$$D = \frac{0.9}{\beta \cos\theta}, \tag{1}$$

where the Bragg diffraction angle is θ, the whole width at half maximum of the XRD peak is β, and the X-ray wavelength is λ.

Table 1 Particles grain size before and after Zn:Cu addition

Samples	Plan (*hkl*)	Position of peak (º)	β(º) FHWM	Grain size (nm)
DD3 (1300 ºC)	(101)	21.67	0.21	38.1
	(210)	26.32	0.29	27.6
	(121)	40.90	0.24	35.2
DD3 + ZnO (28%) + CuO (2.8%)	(101)	21.72	0.36	22.4
	(210)	26.38	0.59	14.2
	(121)	40.97	0.36	23.5
DD3 + ZrO_2 (1300 ºC)	(101)	26.99	0.17	47.5
	(200)	28.22	0.22	37.6
	(112)	35.65	0.23	36.4
DD3 + ZrO_2 + ZnO (28%) + CuO (2.8%)	(101)	27.01	0.35	23.3
	(200)	28.23	0.38	21.6
	(112)	35.65	0.65	13.2

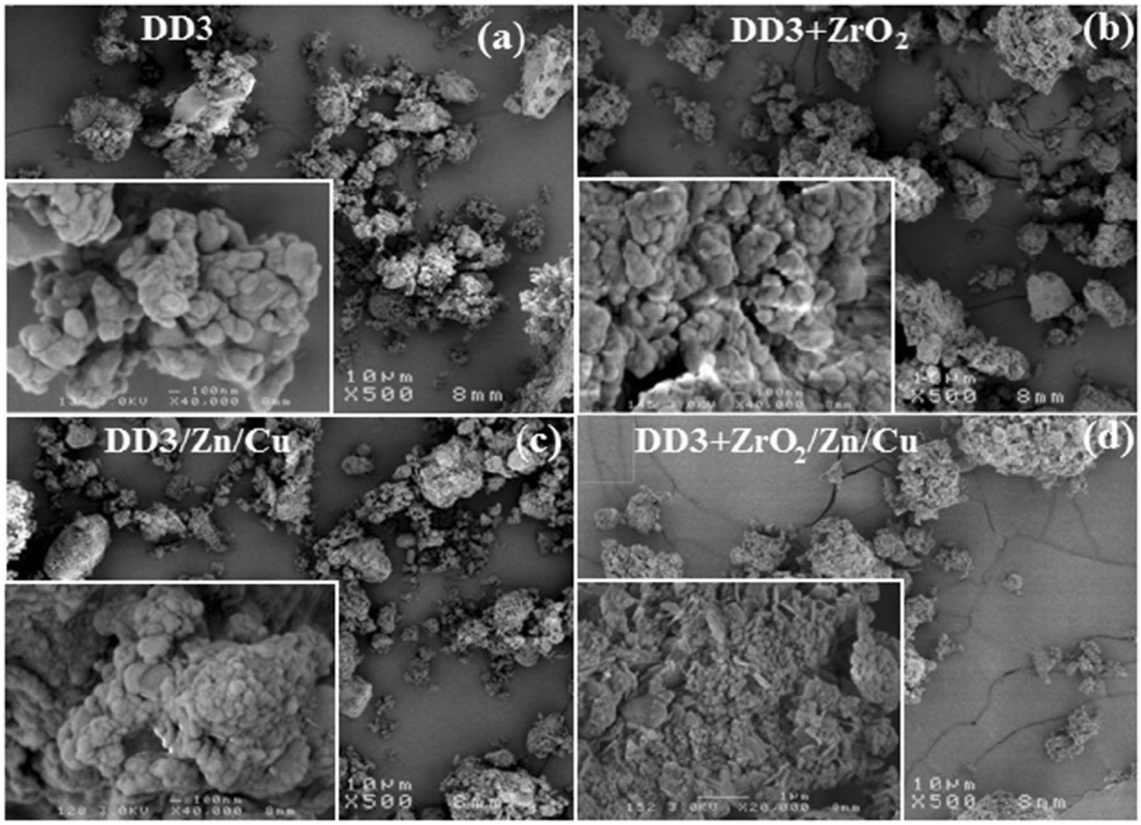

Fig. 4 SEM images of **a** DD3 at 1300 ℃, **b** DD3 + ZrO_2 at 1300 ℃, **c** DD3 + Zn (28%)/Cu (2.8%) composite, and **d** DD3 + ZrO_2/Zn (28%)/Cu (2.8%) composite

3.2 SEM microscopy and EDX spectrometry

The SEM images of the nanoparticle–ceramic material composites obtained by the co-precipitation method are shown in Fig. 4. The images provide evidence of the morphological differences between the two types of powders: the ZrO_2-containing powder has larger, rounded grains with visible micropores throughout its entire surface (Fig. 4a, b); in contrast, the DD3 powders have grains that appear to have no surface porosity (Fig. 4a). The difference between the two types becomes even more noticeable when Zn/Cu is added.

It can be clearly seen that the quantity of ZnO (28%) and CuO (2.8%) attached to the surface of the DD3 is weak (Fig. 4c). However, an increasing amount of ZnO crystallites covers the DD3 + ZrO_2 surface and the morphology is more like flake structures (Fig. 4d). ZnO nanorods were broken up by CuO inclusion, which altered their dimensional characteristics. This change in ZnO shape showed how the concentration of Cu^{2+} ions has a major impact on the rate at which ZnO nanomaterials crystallize.

According to Khalida Mubeen et al. [30], ZnO's form was altered by the addition of CuO. The SEM pictures demonstrate how the various-sized nanorods and flakes are tightly clustered together with tiny spaces and cavities between the grains. Because the CuO nano-flakes packed into the gaps inside the ZnO nanostructure, the size of the nanostructures shrank [30].

The surface morphology of CuO nanoparticles of V. Usha et al. [31] demonstrates that leafy grains make up the CuO nanoparticle's surface morphology. During the annealing process, these grains tend to clump together by absorbing energy from the surrounding environment. The partial transformation of the leaf-like grains into a structure resembling a flower at specific locations is clearly seen in the SEM image. Grain sizes are typically in the range of a few microns [31]. SEM images of ZnO particles produced by Jung-Hwan Lee et al. [32] revealed the following shapes: a 30 nm spherical particle; a short, thick needle; a comparatively thin, long needle; a small hexagonal planar form; and a large planar.

Figure 5 shows the peaks due to the elements Al, Si, Zr, and O, which allows us to assume that they are mullite–cristobalite (Fig. 5a) and mullite–zircon (Fig. 5b). The carbon signals that appeared in the EDX spectra were attributed to the carbon coating on the device grid.

Figure 5c, d confirms by EDX analysis the presence of Zn and Cu in the chemical composition of the ceramic samples (Al, Si, Zr, and O) with more Zn (corresponding atomic percentage 7.41%) for the composite (DD3 + ZrO_2/Zn/Cu).

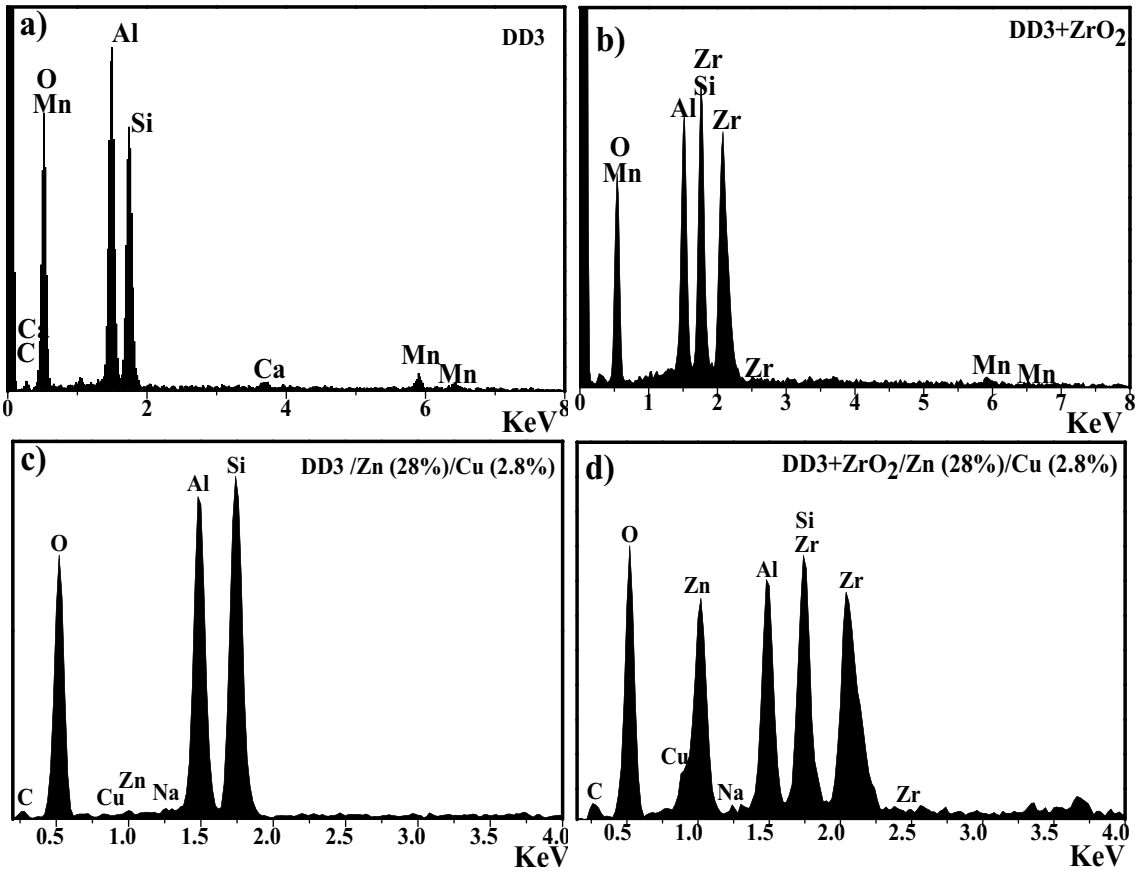

Fig. 5 EDX spectra of a selected area of studied samples

Moreover, the presence of Na reveals the impact of the sample preparation technique. This compound was added during the preparation of the powder to facilitate the dissolution of the zinc and copper acetate. These spectra show distinctive peaks of additional impurities (Mn, Ca), indicating the production of non-pure materials.

The composition of ZnO/CuO measured in these composite was (12.82%/1.08%) and (24.59%/1.49%) for samples DD3/Zn (28 wt%)/Cu (2.8 wt%) and DD3 + ZrO2/Zn (28 wt%)/Cu (2.8 wt%). These are less than the mixture that was employed in the synthesis. It could result from an uneven composite synthesis procedure, like a stirring treatment [33]. Table 2 shows the analysis values that vary according to the concentration and addition ratio.

It has been shown in previous work that adding 38 wt% ZrO_2 to DD3 clay gives the highest porosity rate (33%) on the ceramic surface [22, 25]. The effect of the pores was important in the mechanism of deposition of the added elements, as more zinc was detected in the presence of the pores (Table 2). The percentage of zinc in DD3 + Zn (28 wt%)/Cu (2.8 wt%) is 12.82%, while in the powder containing zirconium oxide (DD3Z + Zn (28 wt%)/Cu

Table 2 Effect of Zn/Cu addition on the chemical composition of thin layers

Samples	Elements (%)								
	O	Al	Si	Zr	Mn	Ca	Na	Zn	Cu
DD3	59.98	11.43	16.18	–	0.86	0.26	–	–	–
DD3 + ZrO_2	75.98	10.83	7.96	4.52	0.71	–	–	–	–
DD3 + Zn (28 wt%)/Cu (2.8 wt%)	60.36	11.07	14.52	–	–	–	0.36	12.82	1.08
DD3 + ZrO_2/Zn (28 wt%)/Cu (2.8 wt%)	54.06	7.09	7.17	5.24	–	–	0.36	24.59	1.49

(2.8 wt%)), the percentage of zinc increases to 24.59%. This means that the amount of material deposited within the small pores led to this significant increase. Therefore, when the microporosity increases, the amount of additive is greater, allowing for better antibacterial activity.

3.3 TEM microscopy

To get a better and more specific view of the internal structures of the material granules, they were examined using SEM in Fig. 6a, which reflects that the kaolinite has a cylindrical structure and the nanotubes are hollow inside, these

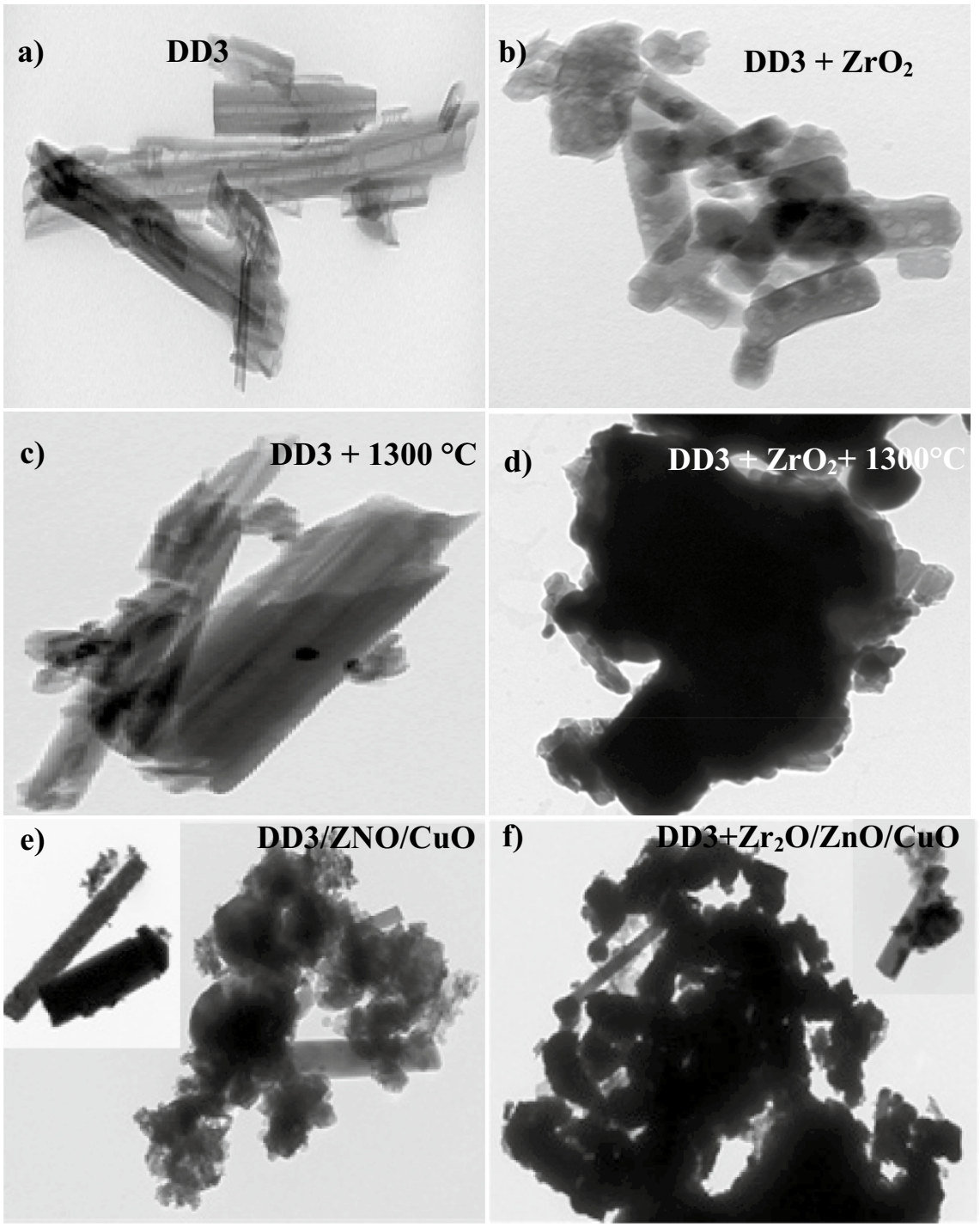

Fig. 6 TEM images of **a** clay DD3, b) clay DD3 + ZrO_2, **b** DD3 treated at 1300 ºC, **d** DD3 + ZrO_2 treated at 1300 ºC, **e** DD3 + Zn (28%)/Cu(2.8%), and **f** DD3 + ZrO_2/Zn (28%)/Cu (2.8%)

cavities extend along the axes of the tubes with open flanges. Zircon oxide (ZrO_2) was added to the adhesion of their nanoparticles to the kaolinite walls (Fig. 6b).

Despite the heat treatment at 1300 ºC for the two types, the tubes largely kept their shape in the first type (Fig. 6c). However, their size decreased (Fig. 6d) due to their disintegration due to the interaction of silica (SiO_2) with ZrO_2 and the emergence of a new compound, which is zircon ($ZrSiO_4$). It can be said that the hollow tubular structure of kaolinite contributed greatly to having a better bacterial effect also because its percentage is the largest in the materials used, with stimulation of additives from zinc and copper oxides (Fig. 6e, f).

The structure and morphology of the crystal The CuO–ZnO sample's TEM analysis was further assessed by Aklilu Guale Bekru et al. [34]. The created CuO–ZnO NCs have plate-like nanostructures, as demonstrated by the results, which validate the SEM investigation.

Surface designs consisting of nanostructures play an important role in inhibiting and reducing bacterial adhesion when bacteria are deposited on the surface terrain. This may lead to putting pressure on the bacterial cell membrane, thus tearing it apart and causing the bacteria to decompose and die by mechanical action [35]. Adhesion behaviors on a surface are strongly determined by surface chemical properties such as surface charges, topologies such as surface roughness, and geometry.

Materialism surfaces that use appropriate topography are promising for disrupting biofilm growth. Ionic surfactants with strong ionic solvents can bind water molecules firmly and stably through electrostatic interaction, which can form a stable and dynamic wetting layer. For example, T. S. Heckmann et al. [36] developed a TiO_2 nanopillar, which endowed the TiO_2 surface with excellent topographical effects resulting from the modification of both organic protein and bacterial contaminants. This topographical effect, which depended largely on the relative size of the detritus, had an enhancement on both global and local shear stress to interfere with bacterial proliferation. Another study suggested that smaller particle sizes may be more effective in reducing bacterial adhesion for both Gram-positive bacteria (e.g., *Staphylococcus aureus*) and Gram-negative bacteria (e.g., *Pseudomonas putida*). Some oxide nanoparticles, SiO_2, CuO, and TiO_2, with low surface energy, have also been used to produce superhydrophobic surfaces, which can trap a stable air layer, thus reducing the contact area between the material and the liquid to prevent bacterial adhesion [37]. It can be said that structured micro-topographic surface patterns with nano-roughness are also able to reduce biofilm formation of bacterial contaminants and thus increase antibacterial activity.

3.4 Raman spectroscopy

Raman spectroscopy is widely used to study the microchemical properties and defects of particles. Through its spectrum, it is also easy to detect secondary phases of possible impurities that cannot be detected by X-ray analysis.

Raman spectra of different area of DD3, DD3Z, DD3/28 wt% ZnO/2.8 wt% CuO and DD3Z/28 wt% ZnO/2.8 wt% CuO are shown in Fig. 7. It has been reported that mullite Raman signature could be observed with a characteristic broad doublet at 250–900 cm^{-1}. All the spectra show Raman bands, particularly around 251, 258, 333, 340, 408, 485, 610, 622, 710, 711, 746, 880, 895, and 899 cm^{-1}. These bands are in accordance with data provided in the literature [38, 39]. The crystallization of mullite leads to the formation of Si–O–Al bonds, which are compatible with 606 and 639 cm^{-1} [40, 41]. The peak due to O–Al–O bond vibration stretching at 143 cm^{-1} is sharp, indicating the development of kaolin in the structure [42, 43].

With the addition of zirconium oxide to kaolin DD3, we notice a complete change in the shape of the spectra and the emergence of peaks of higher intensity. The peak at 800 cm^{-1} corresponds to the Si–O bond vibration in the spectrum of Zircon ($ZrSiO_4$) [44, 45]. There are several Raman bands for ZrO_2 in monoclinic crystal form at 158, 177, 190, 192, 222, 309, 335, 382, 475, 476, 534, 537, 558, 560, 616, and 638 cm^{-1} [46, 47]. The peaks appearing at 214, 230, 394, 425, 485, 554, 757, and 798 cm^{-1} and also the peaks at

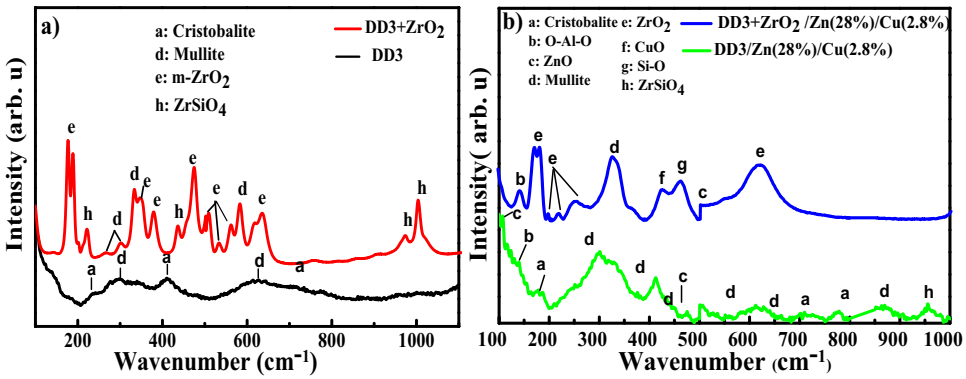

Fig. 7 Raman spectra of sample powders prepared by co-precipitation methods

the interval 40–60 cm^{-1} correspond to cristobalite [48]. The other peaks at 128, 207, 245,264, 354, 464, 467, 589, 640, 664, 697, 808, and 818 cm^{-1} can be attributed to SiO_2 [41]. All spectra for powders in Fig. 7a belong to the millite–cristobalite compound (DD3) and the millite–zircon compound (DD3 + 38 wt%% ZrO_2), and this agrees with the results of the analysis using X-ray.

For powders with the addition of zinc and copper oxide in the traditional mixing method (Fig. 7b), there was a change in the absorption curve in the range [250–1000 cm^{-1}] with an increase in the intensity of the vibration lines to pave the way for the appearance of a very clear ZnO spectrum at 101, 322, 380, 410, 438, 506, 541, 548, 574, 583, 584, and 591 cm^{-1}. It is characteristic of the Zn–O bond vibration [49]. Meanwhile, those at 280, 297, 298, 330, 343, 426, 455, 628, and 632 cm^{-1} are associated with the vibration mode of CuO [50].

3.5 Bacteria test

Three species of bacteria that we had on hand were utilized to test the previously made powders. These bacteria are the most commonly used and employed by researchers because they grow quickly in a suitable medium at 37 °C. The inhibition zone of each ceramic pellet was assessed after 24 h. Table 3 presents the findings.

Our findings further demonstrate the efficiency of the produced materials in creating inhibitory zones. All of the examined microorganisms have the maximum sensitivity to the most concentrated nanomaterials, and more extensive measurements show the zone of inhibition according to the values. This demonstrates that improved antibacterial activity is a function of greater concentration and smaller particle size [51].

For every strain under investigation, it rose following the addition of both copper and zinc. Conversely, the behavior of Gram-positive and Gram-negative strains changed in response to the nanoparticles. While the zone of inhibition for Gram-negative *Escherichia coli* grows and becomes more significant than it would be in the absence of addition, inhibition for Gram-positive *Staphylococcus aureus* exhibits notable symptoms. When it came to fighting bacterial strains, DD3 + ZrO2 and DD3 nanoparticles were less successful than DD3 + ZnO (28%) + CuO (2.8%) and DD3 + ZrO_2 + ZnO (28%) + CuO (2.8%) nanoparticles.

Figure 8 shows the size of the zone of inhibition formed around each disc loaded with test samples, indicating the antibacterial activity towards *S. aureus* and *B. subtilis* for different ceramic compounds.

The rate of inhibition of the biofilm biomass formed by *S. aureus*, *P. aeruginosa*, and *E. coli* in contact with different concentrations of DD3/Zn/Cu and DD3Z/Zn/Cu nano-composites. After adding (28 wt% Zn/2.8 wt% Cu) to the two types of ceramics DD3 and DD3 + ZrO_2, we reach (14.225 ± 0.22 and 24.275 ± 0.27) for *P. putida*, (20.975 ± 0.02 and 38.1 ± 0.1) for *S. aureus* and (13.05 ± 0.05 and 24.9 ± 0.1) for *B. subtilis*, respectively. We note that the percentage of inhibition of biofilm formation of the strains tested is dose-dependent and proportional to increasing concentrations of ZnO/CuO. The zone of inhibition and antibacterial activity surrounding the DD3 is depicted in Fig. 9, both without and with the addition of ZrO_2, Zn, and Cu loaded with test samples.

The amount of work being done toward the synthesis and modification of the particles for biomedical applications has led to a significant advancement in the utilization of inorganic nanoparticles. Microorganisms are poisonous to a variety of heavy metals and metal oxides, either in their free form or as compounds at extremely low concentrations [52].

Through a variety of processes, including attaching to and inactivating intracellular proteins, producing reactive oxygen species, and directly damaging cell walls, these inorganic compounds kill bacteria. Among the most widely utilized inorganic materials, antimicrobial substances are zinc oxide (ZnO), copper oxide (CuO), magnesium oxide (MgO), titanium dioxide (TiO_2), and silver (Ag) [53].

Table 3 Correlation of the size and the inhibition zones of materials

Materials		Bacteria		
		Inhibition zone of materials (mm)		
		P. putida	*S. aureus*	*B. subtilis*
1	DD3	13.1 ± 0.1	23.025 ± 0.07	22.33 ± 0.32
2	DD3 + ZrO_2	11.475 ± 0.47	16.775 ± 0.22	–
3	DD3 (1300 °C)	14.275 ± 0.27	27.8 ± 0.2	23.67 ± 0.32
4	DD3 + ZrO_2 (1300 °C)	16.5 ± 0.5	20.9 ± 0.1	14.15 ± 0.87
5	DD3 + ZnO (28%) + CuO (2.8%)	14.225 ± 0.22	20.975 ± 0.02	13.05 ± 0.05
6	DD3 + ZrO_2 + ZnO (28%) + CuO (2.8%)	24.275 ± 0.27	38.1 ± 0.1	24.9 ± 0.1
7	DD3 + ZrO_2 + ZnO (14.28%) + CuO (5.37%)	29.2 ± 0.2	37.25 ± 0.25	28.85 ± 0.15
8	DD3 + ZnO (14.28%) + CuO (5.37%)	19.25 ± 0.25	32.525 ± 0.47	24.12 ± 0.12

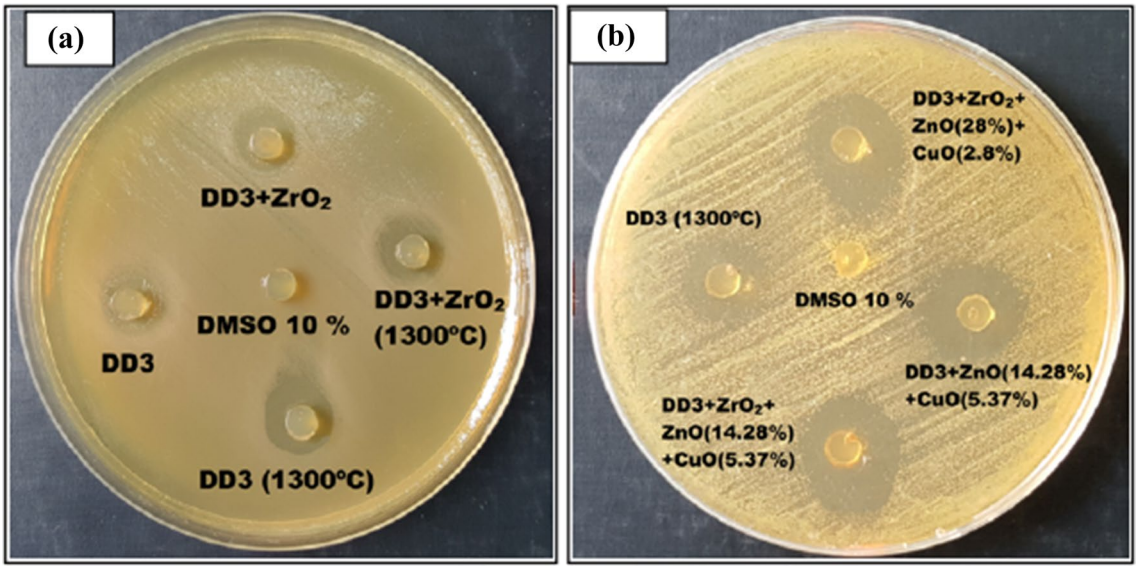

Fig. 8 Results of the halo test of **a** *S. aureus* and **b** *Pseudomonas* after incubation at 37 °C for 24 h

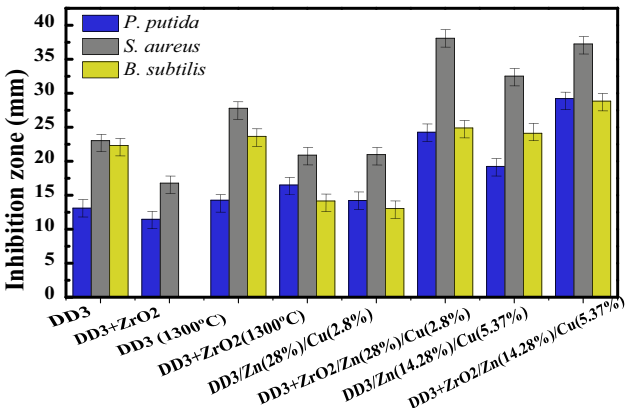

Fig. 9 Changes in the inhibition zone of materials during the use of prepared ceramic compounds. Results are the means of triplicate. Values from bars with the same letter do not differ statistically (LSD)

Ahmad and Kalra [54] observed that ZnO NPs prepared biologically from ethanolic extract of Euphorbia hirta leaves at different concentrations of 20, 40, 60, and 100 µg/ml caused growth inhibition of *Escherichia coli* with inhibition zones of 12, 16, 20, and 24 mm, respectively. ZnO and CuO nanoparticles were prepared by Rania Dadi et al. [55] to see their antibacterial activity on *Staphylococcus aureus*, *Escherichia coli*, and *Pseudomonas aeruginosa*.

The sol–gel method was used to prepare samples. The results obtained showed that the inhibition of bacteria by CuO nanoparticles is more effective than ZnO. Based on the findings of R. Britto Hurtado et al. [56], copper nanoparticles (CuNPs and CuONPs) were prepared using the green synthesis method, which is an effective alternative to traditional physical and chemical methods. It also showed its effectiveness when applied as an antibacterial agent for the organisms that cause microbes and diseases. The results obtained by Jing Kong et al. [57] examined the antibacterial activity of Cu_2O/ZnO composite on two strains of Gram-positive (*S. aureus*) and Gram-negative (*E. coli*) bacteria. A decrease in cocci growth was observed when more than 5% Cu_2O stimulants were added under visible light within 30 min of treatment. In comparison, the antibacterial activity of Cu_2O/ZnO is 2.7 times higher than pure ZnO and kills bacteria in *E. coli* [57] (see Table 4).

3.6 Antibacterial test

In the present study, 8 types of materials synthesized from Mullite, zircon, cristobalite, zinc, and copper were tested against three strains of pathogenic bacteria *P. putida*, *B. subtilis*, and *S. aureus*. These bacteria have been reported to be agents causing human diseases. In addition, multiple drug-resistant *S. aureus* (MRSA) bacteria have significantly increased nowadays [61].

Antibacterial activity results showed that, except for sample 6, which did not affect *Bacillus*, the other samples exhibited activities against all tested bacteria, whether Gram-positive or negative. The physical characteristics of the bacterial cell wall, including its thickness, density, porosity, and integrity, as well as its chemical makeup, determine how different two bacterial groups are from one another. While Gram-negative bacteria have thin walls encircled by lipid-rich membranes, Gram-positive bacteria have thick, dense, comparatively non-porous walls and retain the primary colors.

Table 4 Results of antibacterial activity of some previous works

Antibacterial activity	Synthesis method	Treatment	Inhibition zone (mm)			References
			P. putida	*S. aureus*	*B. subtilis*	
ZnO nanoparticles	Plant material	–	24	29	–	[51]
ZnO and CuO nanoparticles	Sol–gel method	60 °C	38 for CuO, 30 for ZnO	31 for CuO, 28 for ZnO	–	[52]
CuO nanoparticles (NPs)	Mechanochemical method	60 °C	10.6 and 11.2	11.3 and 12.4	–	[58]
ZrO_2 nanoparticles	Sol–gel method	4 °C and 25 °C	1.25	–	–	[59]
ZrO_2–Ag_2O nanoparticles	Sol–gel method	500 ºC	15 ± 1.6	16 ± 0.3	17 ± 1.4	[60]
DD3 + ZrO2/Zn/Cu	Co-precipitation method	500 ºC	24.27 ± 0.27	38.1 ± 0.1	24.9 ± 0.1	Current work

Table 5 Value of DD3 activity based on the other samples

DD3	Percentage increase (%)						
Samples	2	3	4	5	6	7	8
S. aureus	27.15	20.76	9.20	8.90	65.5	61.81	41.27

The values of inhibition zones are shown in Table 5. By comparing these values, it could be observed that those obtained by samples 6 and 7 were larger than (24–29) mm for *P. putida,* (37–38) mm for *S. aureus,* and (24–28) mm for *B. subtilis*) those obtained with the other samples (1, 2, 3, 4, 5, and 8). Samples 6 and 7 are composed of DD3 + ZrO_2, ZnO, CuO with different percentages: (DD3 + ZrO_2 + ZnO (28%) + CuO (2.8%), DD3 + ZrO_2 + ZnO (14.28%) + CuO (5.37%)). *S. aureus* was the most sensitive strain (38.1 ± 0.1) mm. Several studies have reported the antibacterial activity of nanoparticles of ZnO, CuO, and ZrO_2 [18, 19, 24, 62]. It was found that ZnO and CuO nanoparticles exhibit antibacterial activity, and this antibacterial activity increases with the decreasing size of these nanoparticles.

This decrease in the size of the nanoparticles is due to the methods of preparation and heat treatment used. Also, ZnO and CuO nanoparticles contribute to the greater mechanical damage of the cell membrane [63] and their enhanced bactericidal effects. Antimicrobial and antifungal studies revealed that a zirconia nanoparticle shows that the active surface plays a vital role in defining the activity against microbes. Numerous biomedical applications of therapeutic importance show how they counteract colon cancer and highly resistant microorganisms as well.

Interestingly, it is pointed out that DD3, without the addition of ZrO_2, ZnO, and CuO, also presented an antibacterial activity (sample 1) against all strains tested. The relative increase in region value after adding the oxides to the DD3 is shown in Table 3 for one type of *Staphylococcus aureus* bacteria (Fig. 10).

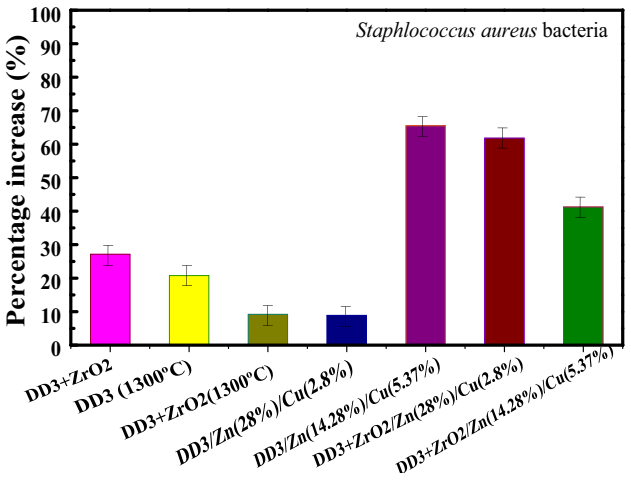

Fig. 10 Effect of the addition on the ceramic DD3 type and its effectiveness against *S. aureus* bacteria

3.7 Penetration of nanoparticles principle

The mechanism of penetration of nanoparticles remains to be elucidated. Indeed, the interaction of physical particles with the bacterial wall has been studied little, and therefore, their penetration into the bacterial wall has been observed little [64]. There are, however, a few possible explanations. The first is that the particles are able to pass through the wall's non-specific porins, but since the largest porins have a diameter of 2 nm, this explanation seems implausible. The second most likely explanation is that the particles are able to exert mechanical pressure on the wall because there is a difference in the concentration of osmolyte on either side of

the membrane, which allows them to force a passage through [65].

However, a measurement of the osmolality of the nanoparticle suspensions was carried out and showed that it is very low. Thus, the nanoparticles do not exert any hyperosmotic pressure and, therefore, cannot force their way through the membrane in this way. The third hypothesis would be that a particle in contact with the membrane could produce ROS and thus cause membrane damage [66]. Holes in the membrane would be formed and allow penetration of the nanoparticles into the periplasm or cytoplasm [67].

The importance of the charge of the particle so that it can approach the wall and release the ROS in its vicinity, the positively charged nanoparticles penetrate the bacterial wall (Fig. 11). Therefore, it is perhaps the charge of the particles, in addition to or in substitution for their size, which conditions the penetration of nanoparticles. Furthermore, this supports the third hypothesis of the penetration mechanism [68].

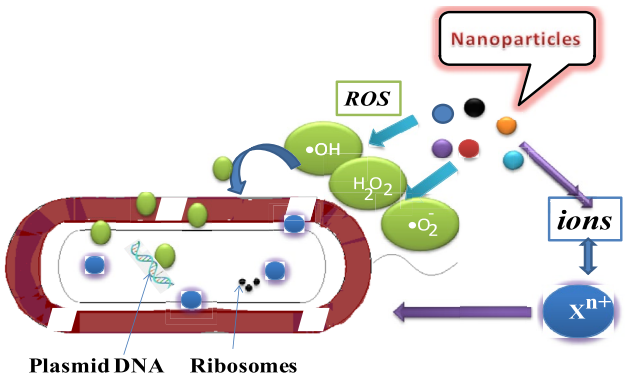

Fig. 11 Principle of antibacterial activity of nanoparticles

3.8 Antibacterial mechanism

The benefits of using these inorganic oxides of nanoparticles as antimicrobial agents include their decreased toxicity and heat resistance, as well as their increased effectiveness against resistant strains of pathogenic origin. The presence of reactive oxygen species (ROS) generated by the nanoparticles of ZrO_2, SiO_2, $ZrSiO_4$, Al_2O_3, ZnO, and CuO is responsible for their bactericidal activity. The nanoparticles' antibacterial behavior may be attributed to hydrogen peroxide and membrane proteins, as the product of hydrogen peroxide penetrates bacterial cell membranes and kills them. Hydrogen peroxide is generated once by DD3/ZnO/CuO and DD3Z/ZnO/Cu. The nanoparticles stay in contact with dead bacteria to prevent the action of the bacteria and further generate and discharge hydrogen peroxide.

The action of Zr^{4+}, Al^{3+}, Si^{4+}, Zn^{2+}, and Cu^{2+} ions on bacteria depends on the genus and species of the microorganism considered; the ions interact with numerous negatively charged groups contained in biological molecules. The metal cations act simultaneously on many sites in the cell. The surface of the particle generates reactive oxygen species (ROS), represented by the $\cdot O_2^-$, ·OH, and H_2O_2 [69], and when the concentration is sufficient, the microorganism cannot mutate before being killed.

The antibacterial performance observed for DD3-clay and DD3 + 38% ZrO_2 modified clay sample is due to the shape and the structure of the specific surface which played an important role in the trapping of holes and electrons by donors (H_2O) and electron acceptors (O_2) respectively and can develop a more active surface of the materials (Fig. 12). The composites of mullite and Zircon products after a high process will be more adapted to generate (electron/hole)

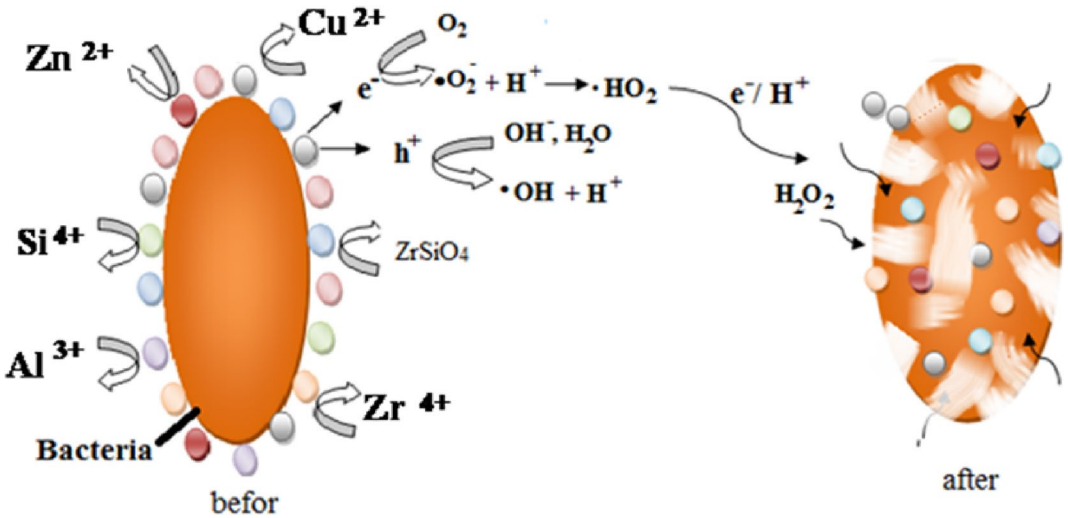

Fig. 12 Antibacterial processes of the composite (ceramic/ZnO/CuO)

[70–72]. This is due to the newly created phase, namely zircon [73].

However, the band gap of this composition (E_g (SiO_2) = (6.1–6.6) eV [74], E_g(Al_2O_3) = 7.4 eV [75], E_g ($ZrSiO_4$) = 6.5 eV [28], E_g(m-ZrO_2) = 3.6 eV [76]) creates small amounts of e^-/h^+ by the photonic radiation absorbance of visible light. When the addition of zinc and copper oxides is added, the combination is avoided, and the number of electrons facilitating the education of cap O sub 2 to, cilitating the education of O_2 to $\cdot O_2^-$ radicals is increased. The $\cdot O_2^-$ may then react with H^+ to form $\cdot HO_2$ and H_2O_2 [77–80].

On the other hand, interacting holes generated by semiconductors (ZnO, CuO, and ZrO_2) with H_2O and OH^- create the largest number of ·OH radicals, which are the main oxidants. This efficiency of the mechanism is only related to the generated of the radicals such as $\cdot O_2^-$, $\cdot HO_2$, ·OH, and H_2O_2 and give free radicals when they interacted with outer cell walls [81]. The H_2O_2 can kill the bacteria by causing deformation, leak, and perturbation when it penetrates the cell membrane of the bacteria [82–84].

When the specific surface area of the active materials is greater, the generation of H_2O_2 is greater, resulting in better antibacterial efficiency.

4 Conclusions

The study describes the development of new ceramics/ZnO/CuO composites with two types of kaolin (DD3 and DD3Z) for their use in the antibacterial activities on two bacterial strains with different Grams due to their extensive involvement in the phenomena of contamination and infection encountered in the medical field. The co-precipitation method was used to produce the samples. The substrates and membranes developed in this study were studied for their structural, morphological, and antimicrobial activity properties. X-ray diffraction analysis indicated that the samples with the addition of metals (Zn:Cu) rose, and the size of the samples decreased between 13 and 24 nm. Surface topography analysis by SEM also confirmed that the ceramic substrates had excellent porous surfaces. A decrease in grain size and surface roughness was observed after the addition of zinc and copper to both types. ZnO and CuO particle existence was verified by scanning electron microscopy and energy dispersive X-ray, which also demonstrated that ZnO particles are deposited onto the surface of ceramic-based mullite–zircon with flake structures. Raman analyses showed distinct vibration for Si–O–Al, O–Al–O, Si–O, Zn–O, and Cu–O bands. The sensitivity of harmful microorganisms to these materials was confirmed by antibacterial tests conducted against Gram-positive (*Staphylococcus aureus* and *Bacillus subtilis*) and Gram-negative (*Pseudomonas putida*) bacteria. The assay identified two potent antimicrobial agents, DD3 + ZrO_2 + ZnO (28 wt%) + CuO (2.8 wt%) and DD3 + ZrO_2 + ZnO (14.28 wt%) + CuO (5.37 wt%), both of which exhibit significant inhibition zones, particularly against *Staphylococcus aureus*. The zone of inhibition for *S. aureus* bacteria reached 38.1 ± 0.1 mm for the first type of powder, while it reached 37.25 ± 0.25 mm for the second type, respectively. In the present study, the ability of a low-cost ceramic material (DD3) to inhibit bacterial growth is reported. The ceramics/ZnO/CuO may be promising agents for antibacterial applications.

Acknowledgements The research has been supported by the laboratory of MOLTECH-Anjou, University of Angers, through a mobility project, PHC Tassili (France). The authors acknowledge the support received from the Researchers Supporting Project (number RSP2024R404), King Saud University, Riyadh, Saudi Arabia.

Declarations

Conflict of interest The authors have no relevant financial or non-financial interests to disclose.

Ethical approval Not applicable.

Consent to participate Not applicable.

Consent to publish Not applicable.

References

1. P. Shree, C. Kant Singh, K. Kaur Sodhi, J. Niranjane Surya, D. Kumar Singh, Biofilms: Understanding the structure and contribution towards bacterial resistance in antibiotics. Med. Microecol. **16**, 100084 (2023)
2. L.M. Streicher, Exploring the future of infectious disease treatment in a post-antibioticera: a comparative review of alternative the rapeutics. JGAR **24**, 285–295 (2021)
3. T. Li, Z. Wang, J. Guo, C. Fuente-Nunez, J. Wang, B. Han, H. Tao, J. Liu, X. Wang, Bacterial resistance to antibacterial agents: Mechanisms, control strategies, and implications for global health. Sci. Total. Environ. **860**, 160461 (2023)
4. F. Dionisio, R. Zilhão, J. Alves Gama, Interactions between plasmids other mobile genetic elements affect their transmission and persistence. Plasmid **102**, 29–36 (2019)
5. C. Zhao, J. Kang, Y. Li, Y. Wang, X. Tang, Z. Jiang, Carbon-based stimuli-responsive nanomaterials: classification and application. Cyborg Bionic Syst. (2023). https://doi.org/10.34133/cbsystems.0022
6. N.T. Hillock, T.L. Merlin, J. Turnidge, J. Karnon, Modelling the future clinical and economic burden of antimicrobial resistance: The feasibility and value of models to inform policy. Appl. Health Econ. Health Policy **20**, 479–486 (2022)
7. L. Zhenxiang, G. Weina, L. Chang, Isolation, identification and characterization of novel *Bacillus subtilis*. Vet. Med. Sci. **80**, 427–433 (2018)
8. J.R. Lakkakula, T. Matshaya, R.W.M. Krause, Cationic cyclodextrin/alginate chitosannanoflowersas 5-fluorouracil drug delivery system. Mater. Sci. Eng. C **70**, 169–177 (2017)
9. O. Ivashchenko, B. Peplińska, J. Gapiński, D. Flak, M. Jarek, K. Załęski, G. Nowaczyk, Z. Pietralik, S. Jurga, Self-organizing silver and ultrasmall iron oxide nanoparticles prepared with ginger

rhizome extract: characterization, biomedical potential and microstructure analysis of hydrocolloids. Mater. Des. **133**, 307–324 (2017)
10. Z. Yu, Q. Li, J. Wang, Y. Yu, Y. Wang, Q. Zhou, P. Li, Reactive oxygen species-related nanoparticle toxicity in the biomedical field. Nanoscale Res. Lett. **15**, 115 (2020)
11. Y. Wang, W. Zhai, S. Cheng et al., Surface-functionalized design of blood-contacting biomaterials for preventing coagulation and promoting hemostasis. Friction (2023). https://doi.org/10.1007/s40544-022-0710-x
12. V.L. Prasanna, R. Vijayaraghavan, Chemical manipulation of oxygen vacancy and antibacterial activity in ZnO. Mater. Sci. Eng. C **77**, 1027–1034 (2017)
13. M. Fellah, N. Hezil, D. Bouras, A. Montagne, A. Obrosov, W. Jamshed, R.W. Ibrahim, A. Iqbal, S.M. El Din, H.A. El-Wahed Khalifa, Investigating the effect of milling time on structural, mechanical and tribological properties of a nanostructured hiped alpha alumina for biomaterial applications. Arab. J. Chem. **16**, 105112 (2023)
14. E. Piktel, Ł Suprewicz, J. Depciuch, S. Chmielewska, K. Skłodowski, T. Daniluk, G. Król, P. Kołat-Brodecka, P. Bijak, A. Pajor-Świerzy, K. Fiedoruk, M. Parlinska-Wojtan, R. Bucki, Varied-shaped gold nanoparticles with nanogram killing efficiency as potential antimicrobial surface coatings for the medical devices. Sci. Rep. **11**, 12546 (2021)
15. B. Dikra, M. Rasheed, R. Barille, M.N. Aldaraji, Efficiency of adding DD3+(Li/Mg) composite to plants and their fibers during the process of filtering solutions of toxic organic dyes. Opt. Mater. **131**, 112725 (2022)
16. B. Rainer, D. Antoine, R.H. Colin, M. Claudine, P.C.R. Eduardo, S. Agnieszka, V. David, *Bacillus subtilis*, the model Gram-positive bacterium: 20 years of annotation refinement. Microb. Biotechnol. **11**, 3–17 (2018)
17. S. Pukird, W. Song, S. Noothongkaew, S.K. Kim, B.K. Min, S.J. Kim, K.W. Kim, S. Myung, K.S. An, Synthesis and electrical characterization of vertically- aligned ZnO–CuO hybrid nanowire p– n junctions. Appl. Surf. Sci. **351**, 546–549 (2015)
18. M.J. Woźniak-Budych, Ł Przysiecka, K. Langer, B. Peplińska, M. Jarek, M. Wiesner, G. Nowaczyk, S. Jurga, Green synthesis of rifampicin-loaded copper nanoparticles with enhanced antimicrobial activity. J. Mater. Sci. Mater. Med. **28**, 42 (2017)
19. W. Wu, W. Zhao, Y. Wu, C. Zhou, L. Li, Z. Liu, J. Dong, K. Zhou, Antibacterial behaviors of Cu_2O particles with controllable morphologies in acrylic coatings. Appl. Surf. Sci. **465**, 279–287 (2019)
20. P. Panchal, R. Sharma, A. Sudharshan Reddy, K. Nehra, A. Sharma, S.P. Nehra, Eco-friendly synthesis of Ag-doped ZnO/MgO as a potential photocatalyst for antimicrobial and dye degradation applications. Coord. Chem. Rev. **493**, 215283 (2023)
21. Y.N. Slavin, J. Asnis, U.O. Hafeli, H. Bach, Metal nanoparticles: Understanding the mechanisms behind antibacterial activity. J. Nanobiotechnol. **15**, 65 (2017)
22. B. Dikra, A. Mecif, R. Barillé, A. Harabi, M. Rasheed, A. Mahdjoub, M. Zaabat, Cu:ZnO deposited on porous ceramic substrates by a simple thermal method for photocatalytic application. Ceram. Int. **44**, 21546–21555 (2018)
23. A. Mftah, F. Halhassan, M.S. El Al-Qubaisi, M.E. Zowalaty, T.J. Webster, M. Sh-eldin, A. Rasedee, Y.-Y. Rasedee, Physicochemical properties, cytotoxicity, and antimicrobial activity of sulphated zirconia nanoparticles. Int. J. Nanomed. **10**, 765–774 (2015)
24. S. Gowri, R. Rajiv Gandhi, M. Sundrarajan, Structural, optical, antibacterial and antifungal properties of zirconia nanoparticles by biobased protocol. J. Mater. Sci. Technol. **30**, 782–790 (2013)
25. D. Bouras, A. Mecif, R. Barille, A. Harabi, M. Zaabat, Porosity properties of porous ceramic substrates added with zinc and magnesium material. Ceram. Int. **46**, 20838–20846 (2020)
26. K. Hassan, R. Hossain, R. Farzana, V. Sahajwalla, Microrecycled zinc oxide nanoparticles (ZnO NP) recovered from spent Zn–C batteries for VOC detection using ZnO sensor. Anal. Chim. Acta **1165**, 338563 (2021)
27. K. Anandhan, S. Harish, R. Thilak Kumar, Effect of morphology on the formation of CdO nanostructures for antibacterial and hemolytic studies. Appl. Surf. Sci. **489**, 262–268 (2019)
28. D. Tan, P. Yuan, F. Dong, H. He, S. Sun, Z. Liu, Selective loading of 5-fluorouracil in the interlayer space of methoxy modified kaolinite for controlled release. Appl. Clay Sci. **159**, 102–106 (2018)
29. R. Singh, K. Verma, A. Patyal, I. Sharma, P.B. Barman, D. Sharma, Nanosheet and nanosphere morphology dominated photocatalytic and antibacterial properties of ZnO nanostructures. Solid State Sci. **89**, 1–14 (2019)
30. X. Li, H. Jiang, N. He, W. Yuan, Y. Qian, Y. Ouyang, Graphdiyne-related materials in biomedical applications and their potential in peripheral nerve tissue engineering. Cyborg Bionic Syst. (2022). https://doi.org/10.34133/2022/9892526
31. V. Usha, S. Kalyanaraman, R. Thangavel, R. Vettumperumal, Effect of catalysts on the synthesis of CuO nanoparticles: Structural and optical properties by sol–gel method. Superlattices Microstruct. **86**, 203–210 (2015)
32. L. Jung-Hwan, L. Gun-Sub, P. Eung-Nam, J. Dong-Hyeon, K. So-Won, L. Hee-Chul, Synthesis of planar-type ZnO powder in non-nano scale dimension and its application in ultraviolet protection cosmetics. J. Mater. **16**, 2099 (2023)
33. C. Kumar, V. Betageri, G. Nagaraju, G.H. Pujar, H.S. Onkarappa, M. Latha, One-pot green synthesis of ZnO–CuO nanocomposite and their enhanced photocatalytic and antibacterial activity. Adv. Nat. Sci. Nanosci. Nanotechnol. **11**, 015009 (2020)
34. A.G. Bekru, L.T. Tufa, O.A. Zelekew, M. Goddati, J. Lee, F.K. Sabir, Green Synthesis of a CuO–ZnO nanocomposite for efficient photodegradation of methylene blue and reduction of 4-nitrophenol. ACS Omega **7**, 30908–30919 (2022)
35. Y.F. Cheng, G.P. Feng, C.I. Moraru, Micro-and nanotopography sensitive bacterial attachment mechanisms: a review. Front. Microbiol. **10**, 17 (2019)
36. T.S. Heckmann, J.D. Schiffman, Spatially organized nanopillar arrays dissimilarly affect the antifouling and antibacterial activities of *Escherichia coli* and *Staphylococcus aureus*. ACS Appl. Nano Mater. **3**, 977 (2020)
37. H. Fan, Z. Guo, Bioinspired surfaces with wettability: biomolecule adhesion behaviors. Biomater. Sci. **8**, 1502 (2020)
38. M. Fellah, N. Hezil, D. Bouras, A. Obrosov, A.S. Mohammed, A.X. Montagne, A. Abd-Elmonem, S.M. El Din, S. Weiß, Structural, mechanical and tribological performance of a nanostructured biomaterial Co-Cr-Mo alloy synthesized via mechanical alloying. J. Mater. Res. Technol. **25**, 2152–2165 (2023)
39. S. Shoval, M. Boudeulle, G. Panczer, Identification of the thermal phases in firing of kaolinite to mullite by using micro-Raman spectroscopy and curve-fitting. Opt. Mater. **34**, 404–409 (2011)
40. M. Ritz, Infrared and Raman spectroscopy of mullite ceramics synthesized from fly ash and kaolin. Miner. Eng. **13**, 864 (2023)
41. Y. Zhao, J. Jing, L. Chen, F. Xu, H. Hou, Current research status of interface of ceramic-metal laminated composite material for armor protection. Jinshu Xuebao/Acta Metallur. Sin. **57**, 1107–1125 (2021)
42. A. Magdy, Y. Fouad, Y. Fouad, M.H. Abdel-Aziz, A.H. Konsowa, Synthesis and characterization of Fe_3O_4/kaolin magnetic nanocomposite and its application in wastewater treatment. J. Ind. Eng. Chem. **56**, 299–311 (2017)
43. S.A. Di Pietro, H.P. Emerson, Y. Katsenovich, T.J. Johnson, R.M. Francisc, H.E. Masond, M. Marpled, A. Sawveld, J.E. Szecsody, Solid phase characterization and transformation of illite mineral

with gas-phase ammonia treatment. J. Hazard. Mater. **424**, 127657 (2022)
44. P. Dawson, M.M. Hargreave, G.R. Wilkinson, The vibrational spectrum of zircon ($ZrSiO_4$). J. Phys. C Solid State Phys. **4**, 240 (2001)
45. Y. Wang, Y. Xu, W. Zhai, Z. Zhang, Y. Liu, S. Cheng, H. Zhang, In-situ growth of robust superlubricated nano-skin on electrospun nanofibers for post-operative adhesion prevention. Nat. Commun. **13**(1), 5056 (2022)
46. C.M. Efaw, J.L. Vandegrift, M. Reynolds, S. Mc, B.J. Murdie, H. Jaques, H. Hu, M.F. Xiong, Hurley, Characterization of zirconium oxides part I: Raman mapping and spectral feature analysis. Nucl. Mater. Energy. **21**, 100707 (2019)
47. M. Yi, Y. Zhang, J. Xu, D. Deng, Z. Mao, X. Meng, X. Shi, B. Zhao, Surface-enhanced Raman scattering activity of ZrO_2 nanoparticles: effect of tetragonal and monoclinic phases. J. Nanomater. **11**, 2162 (2021)
48. M. Farah, M. Fellah, D. Bouras, N. Hezil, A. Becheri, B. Regis, H. Daoud, A. Montagne, T. Alballa, H.A.E. Khalifa, Unraveling the role of sintering temperature on physical, structural and tribological characteristics of ball milled Co28Cr6Mo biomaterial based alloy. J. Eng. Res. (2023). https://doi.org/10.1016/j.jer.2023.10.040
49. B. Hadžić, N. Romčević, D. Sibera, U. Narkiewicz, I. Kuryliszyn-Kudelska, W. Dobrowolski, M. Romčević, Laser power influence on Raman spectra of ZnO(Co) nanoparticles. J. Phys. Chem. Solids **91**, 80–85 (2016)
50. A.S. Zoolfakar, R.A. Rani, A.J. Morfa, K. Kalantar-Zadeh, Nanostructured copper oxide semiconductors: a perspective on materials, synthesis methods and applications. J. Mater. Chem. C. **2**, 5247–5270 (2014)
51. T. Jan, S. Azmat, Q. Mansoor, H.M. Waqas, M. Adil, S.Z. Ilyas, I. Ahmad, M. Ismail, Superior antibacterial activity of ZnO-CuO nanocomposite synthesized by a chemical Co-precipitation approach. Microb. Pathog. **134**, 103579 (2019)
52. I. Khan, K. Saeed, I. Khan, Nanoparticles: properties, applications and toxicities. Arab. J. Chem. **12**, 908–931 (2019)
53. H. Zhang, C. Zhang, Q. Han, Mechanisms of bacterial inhibition and tolerance around cold atmospheric plasma. Appl. Microbiol. Biotechnol. **107**, 5301–5316 (2023)
54. S. Fu, H. Wu, W. He, Q. Li, C. Shan, J. Wang, C. Hu, Conversion of dielectric surface effect into volume effect for high output energy. Adv. Mater. **35**(40), 2302954 (2023). https://doi.org/10.1002/adma.202302954
55. R. Dadi, R. Azouani, M. Traore, C. Mielcarek, A. Kanaev, Antibacterial activity of ZnO and CuO nanoparticles against gram positive and gram negative strains. Mater. Sci. Eng. C **104**, 109968 (2019)
56. R. Britto Hurtado, Y. Delgado-Beleño, C. E. Martinez-Nuñez, M. Cortez-Valadez, M. Flores-Acosta, Chapter 17—Biosynthesis and antibacterial activity of Cu and CuO nanoparticles against pathogenic microorganisms, copper nanostructures: Next-generation of agrochemicals for sustainable agroecosystems. Nanobiotechnol. Plant Prot., 417–452 (2022)
57. J. Kong, S. Zhang, M. Shen, J. Zhang, S. Yoganathan, Evaluation of copper(I)-doped zinc oxide composite nanoparticles on both gram-negative and gram-positive bacteria. Colloids Surf A Physicochem Eng Asp **643**, 128742 (2022)
58. S. Moniri Javadhesari, S. Alipour, S. Mohammadnejad, M.R. Akbarpour, Antibacterial activity of ultra-small copper oxide (II) nanoparticles synthesized by mechanochemical processing against *S. aureus* and *E. coli*. Mater. Sci. Eng. C **105**, 110011 (2019)
59. N. Tabassum, D. Kumar, D. Verma, R.A. Bohara, M.P. Singh, Zirconium oxide (ZrO_2) nanoparticles from antibacterial activity to cytotoxicity: a next-generation of multifunctional nanoparticles. Mater. Today Commun. **26**, 102156 (2021)
60. A.P. Ayanwale, Ad. Jesús Ruíz-Baltazar, L. Espinoza-Cristóbal, S. Yobanny Reyes-López, Bactericidal activity study of ZrO_2-Ag_2O nanoparticles. Dose Response **18**, 1559325820941374 (2020)
61. B.A. Alghamdi, I. Al-Johani, J.M. Al-Shamrani, H.M. Alshamrani, B.G. Al-Otaibi, K.A. Master, N.Y. Yusof, Antimicrobial resistance in methicillin-resistant *Staphylococcus aureus*. Saudi J. Biol. Sci. **30**, 103604 (2023)
62. G. Lee, B. Lee, K.T. Kim, Mechanisms and effects of zinc oxide nanoparticle transformations on toxicity to zebrafish embryos. Environ. Sci. Nano **8**, 1690–1700 (2021)
63. B.L. de Silva, M.P. Abuçafy, E.B. Manaia, J.A. Oshiro Junior, B.G. Chiari-Andréo, R. Cl R Pietro, L. Aparecida Chiavacci, Relationship between structure and antimicrobial activity of zinc oxide nanoparticles: an overview. Int. J. Nanomed. **4**, 9395–9410 (2019)
64. A. Menichetti, A. Mavridi-Printez, D. Mordini, M. Montalti, Effect of size, shape and surface functionalization on the antibacterial activity of silver nanoparticles. J. Funct. Biomater. **14**, 244 (2023)
65. I. Alav, J. Kobylka, M.S. Kuth, K.M. Pos, M. Picard, J.M.A. Blair, V.N. Bavro, Structure, assembly, and function of tripartite efflux and type 1 secretion systems in Gram-negative bacteria. J. Chem. Rev. **121**(9), 5479–5596 (2021)
66. S.N. Mouton, A.J. Boersma, L.M. Veenhof, A physicochemical perspective on cellular ageing. TIBS. **48**, 949–962 (2023)
67. E.A.S. Dimapilis, H. Ching-Shan, R.M.O. Mendoz, L. Ming-Chun, Zinc oxide nanoparticles for water disinfection. Sustai. Environ. Res. **28**, 47–56 (2018)
68. V. Harish, D. Tewari, M. Gaur, A.B. Yadav, S. Swaroop, M. Bechelany, A. Barhoum, Review on nanoparticles and nanostructured materials: Bioimaging, biosensing, drug delivery, tissue engineering, antimicrobial, and agro-food applications. J. Nanomater. **12**, 457 (2022)
69. D. Bouras, M. Fellah, R. Barille, M. Abdul Samad, M. Rasheed, M.A. Alreshidi, Properties of MZO/ceramic and MZO/glass thin layers based on the substrate's quality. Opt. Quantum Electron. **56**, 104 (2023)
70. F. Karkeh-Abadi, H. Safardoust-Hojaghan, L.S. Jasim, W.K. Abdulsahib, A.M. Makarim, M. Salavati-Niasari, Synthesis and characterization of Cu2Zn1.75Mo3O12 ceramic nanoparticles with excellent antibacterial property. J. Mol. Liq. **356**, 119035 (2022)
71. W. Kuang, H. Wang, X. Li, J. Zhang, Q. Zhou, Y. Zhao, Application of the thermodynamic extremal principle to diffusion-controlled phase transformations in Fe-C-X alloys: modeling and applications. Acta Mater. **159**, 16–30 (2018). https://doi.org/10.1016/j.actamat.2018.08.008
72. D. Bouras, M. Fellah, A. Mecif, R. Barillé, A. Obrosov, M. Rasheed, High photocatalytic capacity of porous ceramic-based powder doped with MgO. J. Korean Ceram. Soc. **60**, 155–168 (2023)
73. M. Amirhossein, Z. Mohammadamin, M.T. Mahzad Haji, The effect of zirconium content on in vitro bioactivity, biological behavior and antibacterial activity of sol-gel derived 58S bioactive glass. J. Non-Cryst. **546**, 120262 (2020)
74. T.C. Dakal, A. Kumar, R.S. Majumdar, V. Yadav, Mechanistic basis of antimicrobial actions of silver nanoparticles. Front. Microbiol. **7**, 1831 (2016)
75. A. Maréchal, M. Aoukar, C. Vallée, C. Rivière, D. Eon, J. Pernot, E. Gheeraert, Energy-band diagram configuration of Al_2O_3/oxygen-terminated p-diamond metal oxide-Semiconductor. J. Appl. Phys. **107**, 141601 (2015)
76. B. Dikra, A. Mecif, A. Harabi, R. Barillé, A. Mahdjoub, M. Zaabat, Economic and ultrafast photocatalytic degradation of orange II using ceramic powders. J. Catal. **11**, 733 (2021)
77. J. Li, S. Meng, J. Niu, H. Lu, Electronic structures and optical properties of monoclinic ZrO_2 studied by first-principles local

density approximation + U approach. J. Adv. Ceram. **6**, 43–49 (2017)
78. K. Wang, J. Zhu, H. Wang, K. Yang, Y. Zhu, Y. Qing, J. He, Air plasma-sprayed high-entropy (Y0.2Yb0.2Lu0.2Eu0.2Er0.2)3Al5O12 coating with high thermal protection performance. J. Adv. Ceram. **11**(10), 1571–1582 (2022)
79. J. Xia, Y. Li, C. He, C. Yong, L. Wang, H. Fu, Y. Zhang, Synthesis and biological activities of oxazolidinone pleuromutilin derivatives as a potent anti-MRSA agent. ACS Infect. Dis. **9**(9), 1711–1729 (2023). https://doi.org/10.1021/acsinfecdis.3c00162
80. R.B. d'Água, R. Branquinho, M. Paula Duarte, E. Maurício, A. Luísa Fernando, R. Martins, E. Fortunato, Efficient coverage of ZnO nanoparticles on cotton fibers for antibacterial finishing using a rapid and low cost in situ synthesis. New J. Chem. **42**, 1052–1060 (2018)
81. S.S. Santosh, K.M. Divya, N.D. Sasikala, V.S. Prakash, M. Vangalapati, Enhanced catalyst performance copper doped ZnO nanoparticles for removal of dicofol. Mater. Today: Proc. **26**, 1718–1722 (2020)
82. N. Ekthammathat, S. Thongtem, T. Thongtem, A. Phuruangrat, Characterization and antibacterial activity of nanostructured ZnO thin films synthesized through a hydrothermal method. J. Powder Technol. **254**, 199–205 (2014)
83. B. Dikra, M. Fellah, R. Barille, S. Weiß, M. Abdul Samad, A. Alburaikan, H. Abd K. El-Wahed, A. Obrosov, Improvement of photocatalytic performance and sensitive ultraviolet photodetectors using AC-ZnO/ZC-Ag_2O/AZ-CuO multilayers nanocomposite prepared by spin coating method. J. Sci. Adv. Mater. Dev. **9**, 100642 (2023)
84. L. Qiao, M.T. Swihart, Solution-phase synthesis of transition metal oxide nanocrystals: morphologies, formulae, and mechanisms. Adv. Colloid Interface Sci. **244**, 199–266 (2017)